Journal of Molecular Catalysis A: Chemical 298 (2009) 88–93

Contents lists available at ScienceDirect

Journal of Molecular Catalysis A: Chemical

journal homepage: www.elsevier.com/locate/molcata

Hydroxyapatite-supported $Rh(CO)_2(acac)$ (acac = acetylacetonate): Structure characterization and catalysis for 1-hexene hydroformylation

Kun Wang*, Gordon J. Kennedy, Raymond A. Cook

Corporate Strategic Research, ExxonMobil Research and Engineering Company, 1545 Rt. 22 East, Annandale, NJ 08801, USA

ARTICLE INFO

Article history:
Received 8 August 2008
Received in revised form 2 October 2008
Accepted 8 October 2008
Available online 17 October 2008

Keywords:
Hydroxyapatite
Supported catalyst
Rhodium
Hydroformylation

ABSTRACT

A high surface area hydroxyapatite [$Ca_{10}(PO_4)_6(OH)_2$] was prepared and used as support for $Rh(CO)_2(acac)$ (acac = acetylacetonate). The supported catalyst (7270 ppm Rh) was characterized using IR and solid state NMR. The proton in the P–OH group of hydroxyapatite reacts with the $acac^-$ ligand forming acetylacetone (acacH); and the Rh dicarbonyl species was anchored on the surface via the resulting $P–O^-$ group. It is proposed that acacH stays coordinated with Rh in the supported catalyst. The supported catalyst is active in catalyzing 1-hexene hydroformylation without the need of an auxiliary ligand such as phosphine [1330 turnovers in 17 h; 300 psig syngas ($H_2/CO = 1$); 100 °C]. Activity for the supported Rh catalyst is an order of magnitude higher than that for un-supported $Rh(CO)_2(acac)$ homogeneous system. The supported catalyst was separated from the reaction medium and re-used; giving a slightly lower activity. This is the only example of $Rh(CO)_2(acac)$ supported on an inorganic material that shows significant activity for olefin hydroformylation without the presence of an auxiliary ligand such as phosphine.

1. Introduction

Supported molecular metal complexes continue to attract significant interest in the field of catalysis [1–3]. The uniformly distributed catalytic species on the surface are regarded as molecular analogues, the structure of which can be determined more precisely than those of supported metal catalysts containing particles or crystallites [3]. In addition, supported molecular catalysts offer advantages such as high selectivity and uniform accessibility (similar to molecular catalysts in solution), as well as ease of separation (characteristic of solid catalysts). Supported molecular catalysts continue to draw interest in the field of olefin hydroformylation and many examples have been reported to-date. Supports such as zeolites [4], amorphous silica-alumina [5], oxides [6], as well as organic polymers [7,8], all have been exploited for hydroformylation catalysts.

Hydroxyapatite [HAP-x, $Ca_{10-x}(HPO_4)_x(PO_4)_{6-x}(OH)_{2-x}$, $x = 0, 1$] is an important class of biomaterial, which is chemically similar to the mineral component of mammalian bones [9]. HAP adopts a hexagonal structure in the $P6_3/m$ space group. The structure can be viewed as consisting of unconnected PO_4^{3-} tetrahedrons with Ca^{2+} in the space between and a chain of OH^- ions along the c-axis to balance the charge [10]. Hydroxyapatites possess a number of interesting properties such as ion-exchange capability, adsorption capacity, acid–base properties, non-toxicity, and thermal stability [9]. These properties make them attractive for catalytic applications. For example, substituting or partially substituting Ca^{2+} (with Ni^{2+} [11] or Cu^{2+} [12]) or P^{5+} (with V^{5+} [13]) makes HAP-type materials active catalysts for a range of reactions. Recently, HAP-supported Pd [14] and Ru [15] made from molecular metal precursors have been reported as efficient catalysts for aerobic oxidation of alcohols.

Using $Rh(CO)_2(acac)$ as precursor for supported Rh catalysts is not new [3]. For example, Wrzyszcz et al. reported $Rh(CO)_2(acac)$ supported on zinc aluminate spinel in a study for olefin hydroformylation [6]. However, no catalytic activity for 1-hexene hydroformylation was observed in the absence of added PPh_3. Here we report the first example using hydroxyapatite as support for rhodium hydroformylation catalyst, its structural characterization and catalysis for 1-hexene hydroformylation.

2. Experimental

2.1. General

All manipulations involving air-sensitive materials were carried out under N_2 either in a dry-box or using standard Schlenk techniques. Solvents (anhydrous grade) were obtained from Aldrich and used as received. Synthesis gas ($H_2/CO = 1$) was purchased from BOC (Murray Hill, NJ). Except for dicarbonylacetylacetonato rhodium(I)

* Corresponding author. Tel.: +1 908 730 2101; fax: +1 908 730 3198.
E-mail address: kun.wang@exxonmobil.com (K. Wang).

1381-1169/$ – see front matter © 2008 Elsevier B.V. All rights reserved.
doi:10.1016/j.molcata.2008.10.012

[$Rh(CO)_2(acac)$, Strem Chemicals], all other chemicals were purchased from Aldrich.

Elemental analysis was obtained by Inductively Coupled Plasma/Atomic Emission Spectroscopy (ICP/AES). BET surface area was measured on a Micromeritics Tristar N_2 sorption instrument employing the ASTM D4365-10 standard method. Powder X-ray diffraction patterns were obtained on a Bruker D4 diffractometer. Transmission IR (Nujol mull) was obtained on a Mattson Sirius100 IR spectrometer.

Magic angle spinning (MAS) ^{1}H NMR spectra were recorded on a 9.4 T Varian InfinityPlus 400 spectrometer corresponding to a ^{1}H Larmor frequency of 400 MHz. Details of the quantitative ^{1}H MAS NMR experimental procedures used are described elsewhere [16]. The ^{31}P MAS NMR spectra were recorded on an 11.7 T Varian InfinityPlus 500 spectrometer corresponding to a ^{31}P Larmor frequency of 202 MHz. The ^{31}P MAS spectra were obtained with a $\pi/4$ rad pulse length, ^{1}H decoupling during acquisition, a recycle delay of 300 s, and averaging 8 scans. All MAS NMR measurements were done at room temperature with samples that were loaded in 4 mm (o.d.) MAS rotors and spun at the magic angle at rates of 10–16 kHz. The ^{1}H and ^{31}P chemical shifts are referenced with respect to external solutions of TMS (δ_H = 0.0 ppm) and 85% H_3PO_4 (δ_P = 0.0 ppm), respectively.

Hydroformylation reactions were carried out in a batch mode in a 70-mL Hastelloy C autoclave fitted with a glass liner and a magnetic stirrer. To avoid possible contaminations, a new glass liner was used for each run. Neat 1-hexene was used as the reaction medium, toward which the catalyst was mixed and loaded into the autoclave inside a N_2-filled dry-box. The autoclave was attached to a gas manifold and purged three times with syngas (H_2/CO = 1), charged with 300 psi of syngas and heated at 100 °C for desired time. The reaction pressure was kept constant by using a large PVT vessel held at a higher pressure (2500 psi) as a gas reservoir. At the end of run, the autoclave was cooled down to room temperature, vented, and catalyst removed before analysis. The liquid products were analyzed by GC (HP 6890 series, HP-5 capillary column, and FID detector) using *n*-decane as the internal standard. Products were identified either using authentic compounds or by GC–MS.

2.2. Material preparation

2.2.1. Preparation of hydroxyapatite $Ca_{10}(PO_4)_6(OH)_2$ (HAP-0)

Stoichiometric hydroxyapatite $Ca_{10}(PO_4)_6(OH)_2$ (HAP-0) was prepared following a modified literature method [15]. In a 1-L three-necked flask fitted with a mechanical stirrer was dissolved 15.75 g of $Ca(NO_3)_2{\cdot}4H_2O$ (66.7 mmol) in 120 mL of de-ionized water and the pH adjusted to 11 with aqueous ammonia. In a separate flask, 5.28 g of $(NH_4)_2HPO_4$ (40 mmol) was dissolved in 150-mL of de-ionized water and the pH adjusted to 11 using aqueous ammonia. Then the $(NH_4)_2HPO_4$ solution was added drop-wise to the $Ca(NO_3)_2$ solution at room temperature via an addition funnel in the course of 30 min with vigorous stirring. The milky mixture was aged in an oven at 105 °C for 30 min, centrifuged, washed four times with copious amount of water. The white solid obtained was dried in an oven at 110 °C overnight. Yield: 6.10 g; Ca/P = 1.6; XRD pattern matches that of a hydroxyapatite standard [17]; BET surface area: 105 m^2/g.

2.2.2. Preparation of supported Rh catalyst on hydroxyapatite using $Rh(CO)_2(acac)$

An amount of 0.063 g of $Rh(CO)_2(acac)$ was dissolved in 65 mL acetone to give a light yellow solution, toward which 2.50 g of HAP-0 was added. The mixture was stirred at room temperature for 5 h and the liquid became colorless. The mixture was filtered; the solid washed with copious amount of acetone and dried under vacuum to give a light yellow solid (yield 2.5 g). ICP/AES reveals the Rh level is 7270 ppm on the hydroxyapatite support.

2.3. 1-Hexene hydroformylation reaction

2.3.1. 1-Hexene hydroformylation using $Rh(CO)_2(acac)$

An amount of 0.0093 g (0.035 mmol) $Rh(CO)_2(acac)$ was dissolved in 20 mL of 1-hexene in a glass liner and loaded into the autoclave. The autoclave was charged with 300 psi of syngas and heated to 100 °C for 17 h; after which the autoclave was cooled down to room temperature and vented. The soluble rhodium catalyst was removed by running the product mixture through a column of silica. The liquid products were analyzed by GC and GC–MS using *n*-decane as an internal standard.

2.3.2. Hydroformylation of 1-hexene using $Rh(CO)_2(acac)$ in the presence of PPh_3

An amount of 0.0093 g (0.035 mmol) of $Rh(CO)_2(acac)$ was mixed with 0.092 g of PPh_3 (0.35 mmol, Rh/P = 1/10), dissolved in 20 mL of 1-hexene in a glass liner, and loaded into the autoclave. The autoclave was charged with 300 psi of syngas and heated to 100 °C for 17 h; after which the autoclave was cooled down to room temperature and vented. The soluble rhodium catalyst was removed by running the product mixture through a column of silica. The liquid products were analyzed by GC and GC–MS using *n*-decane as an internal standard.

2.3.3. 1-Hexene hydroformylation using supported $Rh(CO)_2(acac)$ on hydroxyapatite

An amount of 0.50 g of the supported catalyst (0.035 mmol Rh) was mixed with 20 mL of 1-hexene in the autoclave. The autoclave was charged with 300 psi of syngas and heated to 100 °C for 17 h, after which the autoclave was cooled down to room temperature and vented. The solid catalyst was removed by filtration and the liquid analyzed by GC and GC–MS using *n*-decane as an internal standard.

3. Results and discussion

3.1. Preparation of hydroxyapatite and hydroxyapatite-supported $Rh(CO)_2(acac)$

The chemical composition of hydroxyapatite can be varied from the stoichiometric $Ca_{10}(PO_4)_6(OH)_2$ (Ca/P = 1.67, HAP-0) to the Ca-deficient form $Ca_9(HPO_4)(PO_4)_5(OH)$ (Ca/P = 1.50, HAP-1) by using an appropriate Ca/P ratio during synthesis. ICP/AES analysis of the hydroxyapatite synthesized here reveals a Ca/P atomic ratio of 1.6, suggesting it is close to the stoichiometric form HAP-0. The co-precipitation method employed here generates hydroxyapatite with a BET surface area of 105 m^2/g, which is far greater than that of a commercial sample from Aldrich (22 m^2/g). Adsorption–desorption isotherm of nitrogen at 77 K and the pore size distribution for the hydroxyapatite are given in Fig. 1. The isotherm is similar to the type H1 adsorption isotherm in the IUPAC classification, suggesting the material contains cylindrical pores of nearly uniform size and shape. Pore size distribution (insert in Fig. 1) shows a pore diameter between 10 and 30 nm, with a maximum centered around 20 nm. Scanning electron microscopy (SEM) reveals a granular (0.2 μm × 0.5 μm dimension) morphology for the particles (Fig. 2). Significant peak broadening was observed in the powder XRD pattern (Fig. 3), consistent with the small particle sizes observed in SEM.

The supported catalyst was prepared by stirring the HAP-0 support in an acetone solution containing $Rh(CO)_2(acac)$. Physically adsorbed Rh complex on the surface was washed off

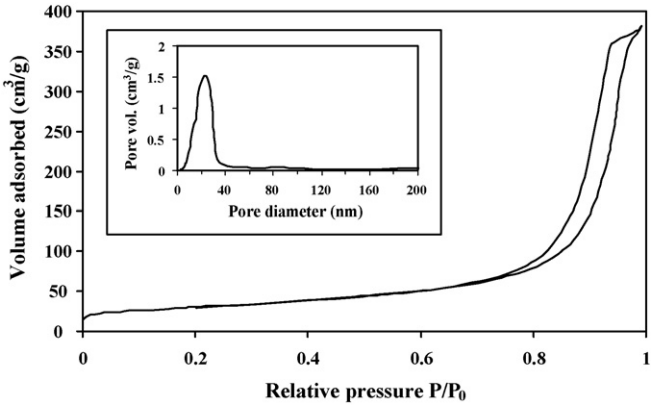

Fig. 1. Nitrogen adsorption–desorption isotherms and pore size distribution for the hydroxyapatite HAP-0.

Fig. 2. SEM image of the hydroxyapatite HAP-0.

using excess acetone. Targeting at 1 wt% rhodium level on HAP-0 using $Rh(CO)_2(acac)$ resulted in a supported catalyst with 7270 ppm Rh. This supported rhodium catalyst is referred as $Rh(CO)_2(acac)$/HAP-0, which was used for characterization and 1-hexene hydroformylation in this study.

3.2. IR characterization of $Rh(CO)_2(acac)$/HAP-0

Since perturbations to the P–OH resonance in IR are too small to be detected due to the very low Rh concentration in $Rh(CO)_2(acac)$/HAP-0, we focused on the carbonyl stretch

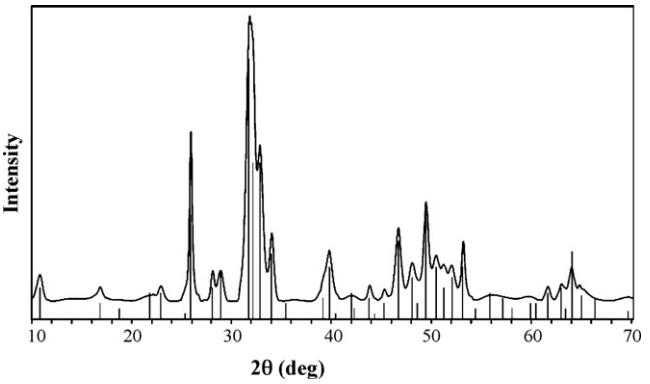

Fig. 3. Powder XRD pattern for the hydroxyapatite HAP-0.

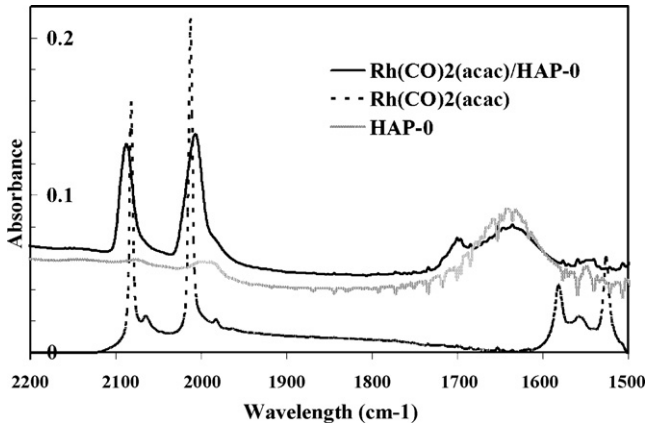

Fig. 4. IR of HAP-0, $Rh(CO)_2(acac)$, and $Rh(CO)_2(acac)$/HAP-0.

region in IR as shown in Fig. 4. Two carbonyl stretches at 2089 cm^{-1} (ν_s) and 2007 cm^{-1} (ν_{as}), respectively were revealed for $Rh(CO)_2(acac)$/HAP-0, consistent with the two carbonyls bound to Rh in a *cis*-fashion [18]. Both peaks are fairly sharp and symmetrical, suggesting the supported catalyst adopts only one major structure. The carbonyl bands observed here are also consistent with those reported for $Rh(CO)_2^+$ supported on $ZnAl_2O_4$ [6] and zeolites [19]. For comparison, two peaks at 2082 cm^{-1} (ν_s) and 2012 cm^{-1} (ν_{as}) are present in $Rh(CO)_2(acac)$. In addition, three resonances (1526, 1557, and 1581 cm^{-1}) in the ketone vibration region were also observed for $Rh(CO)_2(acac)$, which disappear upon supporting on HAP-0, consistent with the $acac^-$ ligand being protonated (by surface P–OH) to acetylacetone (acacH). The weak band around 1700 cm^{-1} in $Rh(CO)_2(acac)$/HAP-0 may be attributed to acacH either bound to Rh or physically adsorbed on HAP-0 surface (free acacH: 1719, 1617 cm^{-1} [17]). Based on the IR results, we propose that the Rh on the supported catalyst is bound to two carbonyls in a *cis*-fashion; and that the $acac^-$ ligand in the precursor is protonated to acacH and stays coordinated to Rh. This proposal for the supported catalyst structure is corroborated by NMR (*vide infra*).

3.3. Solid state NMR characterization of hydroxyapatite-supported $Rh(CO)_2(acac)$

The structure of $Rh(CO)_2(acac)$/HAP-0 was further probed using solid state NMR. Due to the low concentration of Rh relative to the bulk phosphorus, perturbations to phosphorus were undetectable by ^{31}P NMR. By contrast, ^1H NMR readily detects the P–OH group in the HAP-0 support and was used to monitor changes in the supported catalyst (Fig. 5). In addition to the P–OH group (δ_H = 0.3 ppm), ^1H NMR also reveals a broad peak near 7 ppm in HAP-0, which is attributed to residual water. The proton density associated with the P–OH group in HAP-0 is 1.98 mmol/g by ^1H NMR, agreeing with the theoretical value of 1.99 mmol/g for $Ca_{10}(PO_4)_6(OH)_2$, again confirming the hydroxyapatite pre-

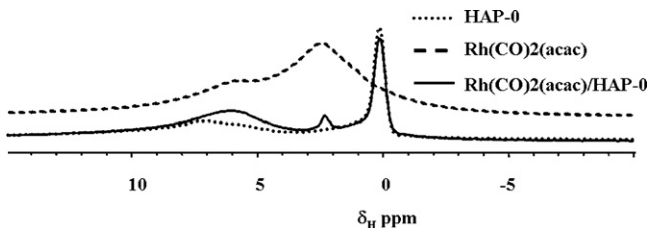

Fig. 5. Solid state ^1H MAS NMR of HAP-0, $Rh(CO)_2(acac)$, and $Rh(CO)_2(acac)$/HAP-0.

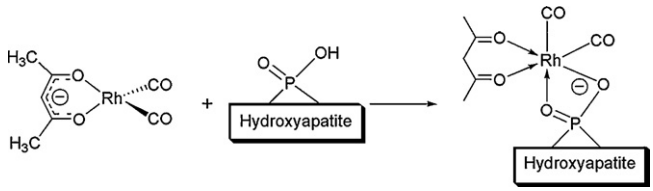

Scheme 1. Proposed formation pathway and structure for $Rh(CO)_2(acac)$/HAP-0.

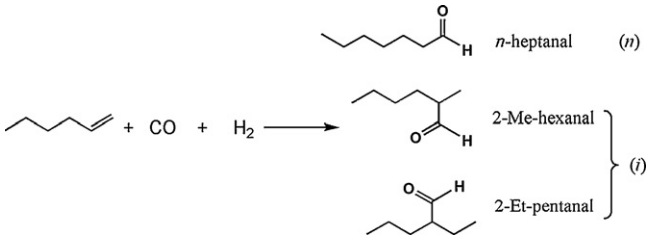

Scheme 2. Aldehyde isomers formed in 1-hexene hydroformylation.

pared here is the stoichiometric form. For $Rh(CO)_2(acac)$/HAP-0, no change in the chemical shift for the P–OH peak is detected; but the concentration of the P–OH group decreases. In addition, a peak at ~2.2 ppm appears. The broad peak associated with residual water in HAP-0 shifts its center slightly upfield, suggesting other proton sources in addition to residual water exist in the supported sample.

The weight-corrected density for the P–OH group decreases from 1.98 to 1.81 mmol/(g HAP-0) upon supporting $Rh(CO)_2(acac)$, suggesting protons associated with the P–OH are partially consumed. Assuming each $Rh(CO)_2(acac)$ reacts with one P–OH, the amount of Rh (7270 ppm) in $Rh(CO)_2(acac)$/HAP-0 would result in a decrease of 0.07 mmol/g in the P–OH density. Although this number is lower than that measured by ^{1}H NMR (0.17 mmol/g), the trends are consistent.

By comparison, solid state ^{1}H NMR of $Rh(CO)_2(acac)$ reveals a broad peak centered around 2.2 ppm ($-CH_3$) and another broad peak around 6 ppm (–CH–). The concentration of protons at 2.2 ppm in $Rh(CO)_2(acac)$/HAP-0 (0.46 mmol H/g) is approximately the same as expected from the $acac^-$ ligand in the $Rh(CO)_2(acac)$ precursor (0.07 mmol Rh/g × 6 H per Rh = 0.42 mmol H/g). We therefore assign the peak at 2.2 ppm in $Rh(CO)_2(acac)$/HAP-0 to the $-CH_3$ groups in acacH, formed via protonation of the $acac^-$ anion by the surface P–OH group. The $-CH_2-$ group in acacH could overlap with the residual water peak, shifting the center of this broad peak upfield. We also acquired ^{13}C CPMAS (cross-polarization magic angle spinning) NMR spectra for both $Rh(CO)_2(acac)$ and $Rh(CO)_2(acac)$/HAP-0, and confirmed the presence of $-CH_3$ on the supported catalyst.

3.4. Proposed formation path and structure of $Rh(CO)_2(acac)$/HAP-0

Based on the characterization results discussed so far, we propose a formation pathway for $Rh(CO)_2(acac)$/HAP-0 (Scheme 1). Upon mixing with HAP-0, the $acac^-$ ligand in $Rh(CO)_2(acac)$ reacts with the proton in the P–OH group on the surface, forming acacH and anchoring the Rh dicarbonyl species $Rh(CO)_2^+$ on the surface via the resulting $P–O^-$ site, with coordination from the P=O group on the same phosphorus atom.

Three possibilities for the fate of the resulting acacH can be considered: (1) as free acacH in solution; (2) physically adsorbed on HAP-0 surface; and (3) coordinated to Rh. After the supported catalyst was filtered, the supernatant in acetone was analyzed by GC/MS. Trace amount of acetylacetone (acacH) was detected. However, free acacH was also observed by GC/MS for a separately prepared $Rh(CO)_2(acac)$ solution (1000 ppm in acetone, similar to the residual level of Rh in the supernatant). Clearly, $Rh(CO)_2(acac)$ decomposes in the GC injector forming acacH. Therefore the acacH observed in the supernatant may very well be due to un-reacted $Rh(CO)_2(acac)$, not necessarily supporting that the existence of free acacH in solution is a result of anchoring as argued by Wrzyszcz et al. [6]. The possibility of physically adsorbed acacH on HAP-0 can also be ruled out. The supported catalyst had been washed extensively with acetone and dried under vacuum for 24 h. Further, the NMR sample had been dried under vacuum at an elevated temperature (50 °C for 10 h). Physically adsorbed acacH (bp 140 °C) is expected to be largely removed after these treatments. Residual acacH left on the surface after these treatments is not expected to give the $-CH_3$ count in ^{1}H NMR matching the Rh concentration in the supported catalyst. Consequently, the most logical proposal is that the acacH stays coordinated to Rh, resulting in a six-coordinated Rh species as shown in Scheme 1.

3.5. 1-Hexene hydroformylation catalyzed by $Rh(CO)_2(acac)$/HAP-0

The hydroxyapatite-supported catalyst $Rh(CO)_2(acac)$/HAP-0 was tested for 1-hexene hydroformylation and the results are listed in Table 1. A total turnover number (TON) of 1330 was achieved using $Rh(CO)_2(acac)$/HAP-0 in 17 h (100 °C, 300 psig, $H_2/CO = 1$, neat 1-hexene). The products contained internal hexenes, *n*-heptanal, 2-methyl-hexanal, and 2-ethyl-pentanal, with an *n*/*i* ratio of 0.8 for the aldehydes [*n*/*i* = *n*-heptanal/(2-Me-hexanal + 2-Et-pentanal); Scheme 2]. For comparison, a homogeneous system containing the same concentration of $Rh(CO)_2(acac)$ (0.035 mmol) alone gave only 167 TON (*n*/*i* = 1.8) under similar conditions, an order of magnitude lower than that of $Rh(CO)_2(acac)$/HAP-0. To gauge the activity of this supported catalyst relative to other rhodium catalysts, a homogeneous $HRh(CO)(PPh_3)_3$ system was generated in situ by mixing $Rh(CO)_2(acac)$ (0.035 mmol) with 10 molar equiv. PPh_3 [20]. Under similar reaction conditions, this Rh/PPh_3 system gave a TON of 3220 (*n*/*i* = 0.9), roughly two and half times that of $Rh(CO)_2(acac)$/HAP-0. Similar *n*/*i*

Table 1
Results for 1-hexene hydroformylation using $Rh(CO)_2(acac)$/HAP-0 ($H_2/CO = 1$, 300 psig, 100 °C, 17 h in neat 1-hexene).

Catalyst	Rh (mmol)	Product composition (mol%)					
		1-hexene	Internal hexenes[a]	*n*-heptanal	2-Me-hexanal + 2-Et-pentanal	TON[b]	*n*/i[c]
$Rh(CO)_2(acac)$	0.035	22	73	3.2	1.9	167	1.8
$Rh(CO)_2(acac)$ + 10 eq PPh_3	0.035	0.8	1.2	46	52	3220	0.9
$Rh(CO)_2(acac)$/HAP-0	0.035	2	69	13	16	1330	0.8
$Rh(CO)_2(acac)$/HAP-0 (re-used)	0.034	6	72	10	12	1040	0.8

[a] Sum of 2-hexenes and 3-hexenes.
[b] Total turnover number (TON) is defined as moles of aldehydes formed per mole of Rh during the total run time.
[c] *n*/*i* = *n*-heptanal/(2-Me-hexanal + 2-Et-pentanal).

ratios were also observed for both $Rh(CO)_2(acac)$/HAP-0 and [$Rh(CO)_2(acac) + PPh_3$], both lower than that for $Rh(CO)_2(acac)$. It is remarkable that the supported catalyst $Rh(CO)_2(acac)$/HAP-0, *without an auxiliary ligand such as a phosphine*, shows activity in the same order of magnitude as that for [$Rh(CO)_2(acac) + PPh_3$]. For comparison, no catalytic activity for 1-hexene hydroformylation was observed in the absence of added PPh_3 for $Rh(CO)_2(acac)$ supported on zinc aluminate spinel [6]. To our knowledge, the work described here is the only example of $Rh(CO)_2(acac)$ supported on an inorganic material that shows significant activity for olefin hydroformylation without the presence of an auxiliary ligand such as phosphine.

At the end of the run, the catalyst $Rh(CO)_2(acac)$/HAP-0 was isolated by filtration. Analysis of the organic solution found 0.95 ppm Rh, indicating 0.3% of Rh leached into solution during the course of reaction. The isolated catalyst was re-used and a TON of 1040 was achieved—slightly lower than that of the fresh catalyst, but still far more active than $Rh(CO)_2(acac)$ alone. The *n*/*i* ratios for the fresh and re-used catalysts were also similar.

The concentration of Rh leached in solution (1.25×10^{-4} mmol Rh) is approximately 300 times lower than the Rh concentration in the $Rh(CO)_2(acac)$ (0.035 mmol Rh) homogeneous system. If the catalytically active species are the same, the amount of Rh leached into solution would contribute a turnover of 0.5, negligible compared to the 1330 TON seen for the supported catalyst. Further, the re-used catalyst shows lower TON (1040), consistent with the catalytically active species being on the support. Thus it is unlikely that the small amount of Rh leached into the solution plays any major role in hydroformylation.

To follow the course of 1-hexene hydroformylation, a large scale reaction was carried out in a 300-mL autoclave ($H_2/CO = 1$, 300 psig, 100 °C, 0.164 mmol Rh, 1.1 mole 1-hexene, for a total of 6 h) and the reaction mixture was sampled periodically. More than 80% of 1-hexene was converted to internal hexenes within the first 30 min, apparently reaching equilibrium after 1 h (Fig. 6a). TON for hydroformylation increased quickly during the first hour, followed by a much slower increase. The initial *n*/*i* ratio was ca. 2.5 but decreased with time (Fig. 6b).

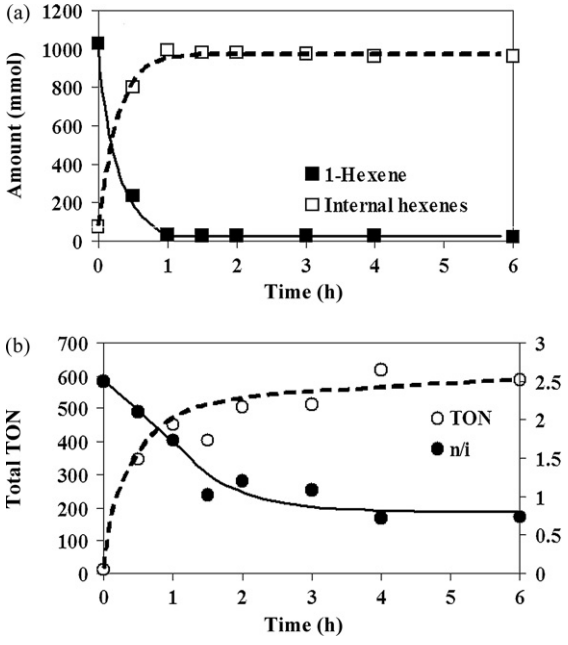

Fig. 6. Behavior of $Rh(CO)_2(acac)$/HAP-0 catalyzed 1-hexene hydroformylation with time: (a) isomerization of 1-hexene; (b) TON and *n*/*i* ratio.

Rhodium-based catalysts are known to be very active for olefin isomerization [21]. Consistently, large amounts of internal hexenes were observed. Although hydroformylation of internal olefins is slower than that for terminal olefins [21], contributions of internal hexenes to the low *n*/*i* ratio (0.8) for $Rh(CO)_2(acac)$/HAP-0 are significant here due to the large amounts of internal hexenes formed, which only give *iso*-aldehydes, reducing the *n*/*i* ratio as reaction time increases.

The low *n*/*i* ratio for $Rh(CO)_2(acac)$/HAP-0 resembles those for simple rhodium compounds [22], suggesting a sterically unhindered coordination environment around Rh, which is consistent with the proposed catalyst structure. Under reaction conditions, the weak coordination of acacH to Rh may dissociate and open up coordination sites for the Rh center for hydroformylation. The higher activity compared to the homogeneous system may be attributed to the effects of the phosphate ligand on the HAP-0 surface. Hydroformylation mechanism on this supported catalyst is not yet clear and will be a topic for future studies.

4. Summary

In summary, a high surface area hydroxyapatite [$Ca_{10}(PO_4)_6(OH)_2$] was prepared and used as support for $Rh(CO)_2(acac)$. The supported catalyst was characterized using IR and solid state NMR. The proton in the P–OH group of hydroxyapatite reacts with the $acac^-$ ligand forming acetylacetone (acacH); and the Rh dicarbonyl species was anchored on the surface via the resulting $P–O^-$ group. It is proposed that acacH stays coordinated with Rh in the supported catalyst. The supported catalyst is active in catalyzing 1-hexene hydroformylation without the need of an auxiliary ligand such as phosphine. Activity for the supported Rh catalyst is an order of magnitude higher than that for un-supported $Rh(CO)_2(acac)$. The supported catalyst was separated from the reaction medium and re-used, giving a slightly lower activity.

Future work will focus on mitigating Rh leaching, understanding the reaction mechanism, and expanding the scope of reaction to other olefins.

Acknowledgments

We thank Mr. C. Chase, Mr. G. Skic, and Mr. D. Colmyer for experimental assistance. Helpful discussions with Drs. D. Stern, D. Calabro, K. Schmitt, M. Afeworki, and S. Rucker are acknowledged.

References

[1] J.-M. Basset, F. Lefebvre, C. Santini, Coord. Chem. Rev. 178 (1998) 1703.
[2] C. Copéret, M. Chabanas, R.P. Saint-Arroman, J.-M. Basset, Angew. Chem. Int. Ed. 42 (2003) 156.
[3] J.C. Fierro-Gonzalez, S. Kuba, Y. Hao, B.C. Gates, J. Phys. Chem. B 110 (2006) 13326.
[4] A. Fuerte, M. Iglesias, F. Sanchez, J. Organomet. Chem. 588 (1999) 186.
[5] J.M. Coronado, F. Coloma, J.A. Andersen, J. Mol. Catal. 154 (2000) 143.
[6] J. Wrzyszcz, M. Zawadzki, A.M. Trzeciak, J.J. Ziolkowski, J. Mol. Catal. A: Chem. 189 (2002) 203.
[7] A. Kocktitz, S. Bischoff, V. Morawsky, U. Prusse, K.-D. Vorlop, J. Mol. Catal. A: Chem. 180 (2002) 231.
[8] G.O. Evans, C.U. Pittman Jr., R. McMillan, R.T. Beach, R. Jones, J. Organomet. Chem. 67 (1974) 295.
[9] J.C. Elliott, Structure and Chemistry of the Apatites and Other Calcium Orthophosphates, Elsevier, New York, 1994.
[10] R. Astala, M.J. Stott, Chem. Mater. 17 (2005) 4125.
[11] M. Misono, W.K. Hall, J. Phys. Chem. 77 (1973) 791.
[12] B.M. Choudary, C. Sridhar, M.L. Kantam, G.T. Venkanna, B. Sreedhar, J. Am. Chem. Soc. 127 (2005) 9948.
[13] S. Sugiyama, T. Osaka, T. Hashimoto, K.-I. Sotowa, Catal. Lett. 103 (2005) 121.
[14] K. Mori, T. Hara, T. Mizugaki, K. Ebitani, K. Kaneda, J. Am. Chem. Soc. 126 (2004) 10657.
[15] K. Yamaguchi, K. Mori, T. Mizugaki, K. Ebitani, K. Kaneda, J. Am. Chem. Soc. 122 (2000) 7144.

[16] G.J. Kennedy, M. Afeworki, D.C. Calabro, C.E. Chase, R.J. Smiley, Appl. Spectrosc. 58 (2004) 698.
[17] http://webbook.nist.gov/chemistry.
[18] R.H. Crabtree, The Organometallic Chemistry of The Transition Metals, 2nd ed., Wiley, New York, 1994, pp. 258–261.
[19] B.E. Hanson, M.E. Davis, D. Taylor, E. Rode, Inorg. Chem. 23 (1984) 52.
[20] Y.S. Varshavsky, T.G. Cherkasova, I.S. Podkorytov, Inorg. Chem. Commun. 7 (2004) 489.
[21] R.H. Crabtree, The Organometallic Chemistry of The Transition Metals, 2nd ed., Wiley, New York, 1994, pp. 223–225.
[22] I. Tkatchenko, in: G. Wilkinson (Ed.), Comprehensive Organometallic Chemistry, Pergamon, New York, 1982, pp. 115–159.